Biochemical and Biophysical Research Communications 450 (2014) 735–740

Contents lists available at ScienceDirect

Biochemical and Biophysical Research Communications

journal homepage: www.elsevier.com/locate/ybbrc

Role of hydrophobic mutations on the binding affinity and stability of blood coagulation factor VIIIa: A computational molecular dynamics and free-energy analysis

Divi Venkateswarlu *

Department of Chemistry, North Carolina Agricultural and Technical State University, Greensboro, NC 27411, USA

ARTICLE INFO

Article history:
Received 21 May 2014
Available online 18 June 2014

Keywords:
Factor VIIIa
Hemophilia-A
Molecular dynamics
MM-PBSA
Binding free-energy

ABSTRACT

Factor VIIIa is a non-covalently bound hetero-trimer among A1, A2 and A3–C1–C2 domains and an essential co-factor for factor IXa enzyme during proteolytic activation of factor X zymogen. The relatively weak interactions between A2 and the interface A1/A3 domains dampen the functional stability of FVIIIa in plasma and results in rapid degradation. We studied the mutational effect of three charged residues (Asp519, Glu665 and Asp666) to several hydrophobic residues by molecular dynamics simulations. Analysis of the binding free energy by MM-PBSA and MM-GBSA methods shows that the mutation of Asp519 and Glu665 residues to either Val or Ala enhance the A2 domain binding affinity in agreement with the experimental site-specific mutagenesis data. Mutation of Asp666 to Val, Tyr, Met and Phe showed largest improvement in the A2-domain binding among the eight hydrophobic mutants studied. Our studies suggest that the enrichment of hydrophobic interactions in the buried surface regions of A2 domain plays crucial role in improving the overall stability of FVIIIa.

1. Introduction

Intrinsic pathway of blood coagulation involves the proteolytic activation of zymogenic factor X (FX) by serine protease IXa (FIXa) in the presence of phospholipids and divalent metal ions [1]. This reaction is catalytically inert and requires the co-factor VIIIa (FVIIIa) association with FIXa [2]. Factor VIII (FVIII) is inactive zymogen that is synthesized as an ~300 kDa single-chain precursor protein with five domains designated as A1–A2–B–A3–C1–C2 [3]. Activation of FVIII by thrombin with proteolytic cleavages at Arg372–Ser373 (A1–A2 junction), Arg740–Ser741 (A2–B junction), and Arg1689–Ser1690 (B–A3 junction) yields activated FVIIIa that circulates in blood as a metal ion dependent non-covalently bound hetero-trimer among A1, A2 and A3–C1–C2 subunits. Deficiency or defect in FVIIIa originates from genetic mutations in certain patient populations due to loss-of-function mutations in the protein. At least 2100 unique mutations have been reported to appear in all domains of FVIII with the clinical severity ranging from mild to severe Hemophilia-A [4]. Currently, there is no cure for hemophilia and the existing therapy includes administration of recombinant FVIII (rFVIII) in Hemophilia patients [5]. However, the existing rFVIII products have short half-lives (~12 h) necessitating frequent intravenous injections to maintain protective FVIII levels in patients [6].

The A2 domain of FVIIIa is weakly bound to the A1 and A3–C1–C2 domains via non-covalent interactions [7]. Such weak interactions contribute to the rapid loss of A2 domain from FVIIIa in the circulating blood plasma and leads to degradation of functional FVIIIa [8]. The accurate structural details of specific residues at the A2 domain interface that contribute to the overall stability of FVIIIa are not well understood due to lack of high quality crystal structures. However, two recently published medium resolution X-ray crystal structures (~3.8 Å resolution) served as the primary source for structural insights into the residues that interface various domains in FVIIIa [9,10]. In order to understand the structure–function relationship of residues that interface A2 domain with other domains, a number of experimental site-specific mutagenesis studies have been reported over the past decade that highlight the residues critical for thermal stability, decay rates and overall cofactor activity of FVIIIa [11,12]. While most of these studies provide details about binding kinetics from experimental approach, the precise structural rationale behind the change in binding affinity is not well known. In this study, we investigated the structural and energetic impact of the mutation of three A2-domain residues, Asp519, Glu665 and Asp666, to several hydrophobic residues by molecular dynamics (MD) simulations and binding free-energy calculations.

* Fax: +1 336 334 7124.
E-mail address: divi@ncat.edu

http://dx.doi.org/10.1016/j.bbrc.2014.06.043
0006-291X/

2. Materials and methods

2.1. Preparation of wild-type FVIIIa (A1A2A3) structure

Based on the 3.8 Å resolution X-ray crystal structure of FVIII (PDB ID: 3CDZ), a full solution structure of FVIIIa was published previously from our laboratory [13]. The activated form of FVIII is a non-covalently bound hetero-trimer among the A1 (Ala1–Arg372), A2 (Ser373–Arg740), A3–C1–C2 (Ser1690–Tyr2332) domains. Since the current work pertains to the study of A2-domain residues that interface A1/A3 domains, to reduce the computational cost, the C1 and C2 domains were removed from the full model of FVIIIa to generate a reduced model of FVIIIa with A1–A2–A3 domains. The full structure of FVIIIa and the reduced model of A1–A2–A3 domains, used in the present study, are presented in Fig. 1. Analysis of the full structure of FVIIIa shows that the C1 and C2 domains are at least 30 Å away from the A2 domain. Therefore, it is reasonable to assume that the removal of C1 and C2 domains would not impact the proposed study of A2 domain mutations. The truncated protein system of A1–A2–A3 domains with the solvated waters was refined for 300 ns of MD simulations. The structure derived from the equilibrate trajectory of the model system, extracted from the 300 ns of MD snapshot, was used for the further study of the proposed mutants.

2.2. Generation of mutant structures

In this work, we report the structure and dynamics of two sets of mutations. The first set comprises of experimentally reported mutation of Asp519 and Glu665 residues of A2 domain with Ala or Val residues. These residues were shown to enhance the binding affinity of A2-domain within FVIIIa complex in several studies [11,12]. The purpose of studying this set of mutations is to validate the accuracy of computational free-energy of binding methods to reproduce the experimental binding affinity data. This provides a proof-of-concept in the application of MM-PBSA and MM-GBSA methods to estimate the binding free-energy of the unknown mutations. The second set of mutants focus on the effect of the mutation of Asp666 residue to several hydrophobic residues. A total of eight hydrophobic mutants were generated where Asp666 was replaced with Tyr, Phe, Trp, Leu, Gly, Ile, Val and Met residues. Each structure was generated by mutating the Asp666 of the WT structure with adjustment of the side-chain torsions using SCREWL rotamer database using CHIMERA graphics software [14]. All mutant structures were solvent-equilibrated and refined for at least 100 ns of explicit-solvent MD simulations.

2.3. Simulation details

All of the proposed structures were modeled in a periodic box with a 12 Å buffer of water molecules explicitly described by the TIP3P model. Initially each simulation system was minimized for 3000 steps by constraining the solute atoms, followed by full minimization of all atoms for 2000 steps to relax the geometry. The first equilibration was carried out with a weak restraint on the backbone solute atoms of the complex for 5000 ps at constant volume, gradually increasing the temperature from 100 to 300 K. The equilibration continued for 5000 ps at a constant pressure of 1 atm by keeping the temperature constant at 300 K with the Langevin temperature equilibration scheme until the density of system reaches to 1.0 g/cc. Under these conditions, the restraints were gradually removed. The production run was carried out without any restraints for 100–140 ns under NVT conditions until the full convergence of the binding free-energy. The convergence test for each simulation is performed on every 200 equally spaced frames, collected over every 10 ns, until the energy becomes consistent for at least four consecutive calculations. A time step of 1 fs was used during the equilibration process, followed by 2 fs time step for production runs. Hydrogen stretching motions were constrained by using SHAKE algorithm. The molecular dynamics simulations were carried out with the AMBER 12 program package using the FF99SB force field and CUDA version of PMEMD with NVIDIA-TITAN GPU graphics cards [15,16]. The analysis of the dynamic trajectories was performed using the *cpptraj* module of AMBER12 program.

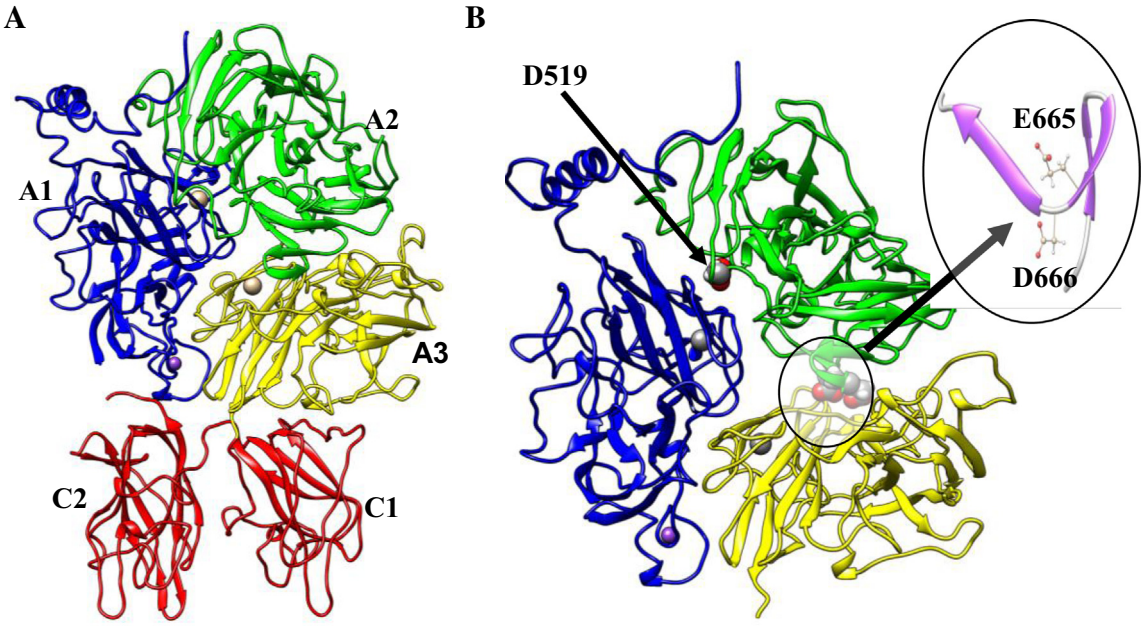

Fig. 1. The full structure of human factor VIIIa (A) and the reduced WT model of A1–A2–A3 domains (B). The C1–C2 domains (in red) were removed for generating WT structure and mutants. The residues Asp519, Glu665 and Asp666 are highlighted. (For interpretation of the references to color in this figure legend, the reader is referred to the web version of this article.)

2.4. Binding free-energy calculations

The A2 domain binding affinity ($\Delta\Delta G_{BIND}$) of the WT and the mutants was calculated based on the molecular mechanics/generalized born surface area (GBSA) and the molecular mechanics/Poisson–Boltzmann surface area (PBSA) approaches. The $\Delta\Delta G_{BIND}$ of A2 domain with A1/A3 domains was calculated as the relative free energy difference between the mutant and WT.

$$\Delta\Delta G_{BIND} = \Delta G_{MUTANT} - \Delta G_{WT}$$

$$\Delta G_{WT} \text{ or } \Delta G_{MUTANT} = G_{A1A2A3} - (G_{A1A3} + G_{A2})$$

The GBSA method is based on the modified GB model developed by Nguyen et al. [17]. The binding free energy consists of the sum of the gas-phase enthalpy (internal, electrostatic and Van der Walls energies) and the solvation free-energy (polar and non-polar) per the equation below.

$$\Delta G_{BIND} = \Delta E_{elec} + \Delta E_{vdw} + \Delta E_{GB} + \Delta E_{SURF}$$

$$\Delta E_{SURF} = (0.0072) \times (\Delta SASA)$$

The PBSA method differs from GBSA where the polar energy contributions are determined by solving the Poisson–Boltzmann equation per the following equation.

$$\Delta G = \Delta E_{vdW} + \Delta E_{ele} + \Delta E_{PB} + \Delta E_{NP}$$

$$\Delta E_{NP} = (\gamma) \times (SASA) + b + G_{disp} \quad (\gamma = 0.0378 \text{ kJ/mol}/A^2 \text{ and } b = -0.5692)$$

A modified version of PBSA method that includes the contribution of dispersion forces to the total free-energy in addition to polar and non-polar solvation terms was used [18]. The setup of solvation parameters are based on the default values as implemented into the *mmpbsa.py* script of Ambertools version 13.0 [19]. All free-energy calculations in the present work were based on 500 snapshots taken every 50 picoseconds from the last 25 ns of MD trajectory for each structure. No entropic corrections were included to the total energy as the studied mutants are at the buried interface between A2 and A1/A3 domains and are expected to have minimal side-chain fluctuations due to constrained conformational space. The small changes in entropy, if significant, may be expected to be canceled out in the estimation of relative free-energies.

3. Results and discussion

3.1. Global structural features of FVIIIa

The reduced model of wild-type (WT) FVIIIa structure was refined for over 300 ns of MD simulations. Analysis of the RMS deviations from the starting conformation shows the full convergence of the structure (Fig. S1a). The backbone aligned structures of five best ranking conformational clusters from the converged MD trajectory show that the protein complex maintains stable interactions most notably at the domain–domain interface between the three regions (Fig. S1b). The time-averaged hydrogen-bonding interactions among the three domains, calculated based on the last 100 ns of simulations, are shown in Table 1 together with the indication of the mutagenic potential of the residues in the H-bond pair that were implicated to be clinically significant [4]. A full list of domain–domain interactions are presented in Table S1. It is evident from the tables that the A2 domain possesses more polar interactions with A1 domain than A3 domain. The A1/A2 domain interface is stabilized by two major ion-pair interactions with Arg282 and Lys496. While Arg282 of A1 domain interacts with Gly520, Pro521 and Asp525 residues with overall H-bond population of >50%, the A2 domain residue Lys496 shares multiple hydrogen bonds with Asp302, Glu354 and Leu303 residues.

Table 1
Hydrogen bonding interactions of A2 domain with A1 and A3 domains in the wild-type FVIIIa structure.

H-bonding		% Population[a]	Mutational severity[b]
A2::A1 domain interactions			
Arg372_NH2	Leu486_O	87	Severe (Arg372)
Thr381_OG1	Gln370_O	32	
Arg484_NH2	Asp361_OD2	61	
Arg484_NH1	Asp361_OD2	54	
Arg484_NH1	Asp361_OD1	32	
Tyr487_OH	Arg372_OXT	39	Severe (Arg372)
Tyr487_OH	Arg372_O	37	
Arg489_NH2	Glu354_OE2	68	
Arg489_NE	Glu354_OE1	48	
Arg489_NH2	Glu354_OE1	31	
Arg490_NH2	Glu354_OE2	42	
Arg490_NE	Glu354_OE2	29	
Arg490_NH1	Asp302_OD1	26	
Val517_O	Arg282_NH2	65	
Gly520_O	Arg282_NH1	87	
Asp525_OD1	His281_NE2	74	Moderate (Asp525)
Met539_O	Ser313_N	38	
Glu540_OE1	Ser313_OG	46	Severe (Glu540)
Glu540_OE2	Ser313_OG	32	
Ser674_OG	Glu287_OE1	35	Moderate (Ser674)
Ser674_OG	Glu287_OE2	30	
Ser695_OG	Leu894_O	41	Moderate (Ser675)
A2::A3 domain interactions			
Lys661_O	Lys1967_NZ	94	Mild (Lys1967)
Glu665_OE1	Arg1966_NH1	58	Severe (Arg1966)
Glu665_OE2	Arg1966_NH2	45	
Glu665_OE2	Arg1966_NH1	34	
Glu665_OE1	Arg1966_NH2	27	
Asn684_OD1	Arg1803_NH1	47	Severe (Asn684)
Pro685_O	Arg1803_NH2	87	Severe (Pro685)
His693_NE2	Gly1981_O	38	Severe (Gly1981)

[a] Hydrogen-bonds with >25% of population are considered as potential interactions.
[b] Mutational data from HAMSTeRS database [4]. Clinical severity of the mutation of residues for which the data is available is listed in parenthesis.

The buried surface area (BSA) among the three domains was computed using NACCESS program [20]. The calculations revealed that the BSA between the A1 and A2 domains is ~3130 Å^2 while that between A2 and A3 domains is 2665 Å^2, suggesting that the A1 and A2 domains have much larger interacting surface area than that between A2 and A3 domains. Inspection of the A2/A3 domain interface shows that it is largely dominated by hydrophobic interactions (Table S2). In order to evaluate the relative energetic contribution of each domain within the A1A2A3 complex, we estimated the binding-free energy of A1 and A2 domains with A2/A3 and A1/A3 respectively. The $\Delta\Delta G_{BIND}$ calculation by GBSA method predicts that the binding affinity of A1 domain with A2/A3 domains is −148 kcal/mol while that of A2 domain with A1/A3 domains is −138.6 kcal/mol. Similarly, the A3 domain affinity with the combined A1/A2 interface is −107.9 kcal/mol. This data suggests that the A3 domain maintains weaker inter-domain interactions with A1/A2 interface. Taken these observations together, it is apparent that the inherent instability of A2-domain within FVIIIa could be largely attributed due to the weak interactions with A3-domain. Thus, it is prudent to infer that stabilizing the A2/A3 binding interface may be critical for improving the overall stability of FVIIIa.

3.2. Validation of computational binding free-energy by GBSA and PBSA

The reliability of the relative free-energies of binding ($\Delta\Delta G_{BIND}$) in proteins estimated by computational MM-GBSA and MM-PBSA

Table 2
Components of the relative binding free energy of A2 domain of the mutant structures as calculated using the MM-PBSA methodology. All values are relative to the corresponding values of the wild-type complex in kcal/mol.

Mutant	$\Delta\Delta G^{GBSA}$	$\Delta\Delta G^{PBSA}$	$\Delta\Delta E_{Gas}$	$\Delta\Delta E_{NP}$	$\Delta\Delta E_{PB}$	$\Delta\Delta E_{DISP}$
D666L	−21.4	−45.6	−388	−17.0	325.9	33.0
D666Y	−35.0	−36.3	−223	−15.0	177.4	23.6
D666M	−1.5	−22.7	−309	14.0	11.4	−23.8
D666F	−16.0	−20.9	−8	−3.7	−10.6	−1.5
D666G	−4.2	−8.7	−149	9.8	149.2	−18.5
D666W	−19.4	−5.5	−176	−5.0	154.8	20.5
D666I	2.1	7.1	−18	9.4	29.7	−13.1
D666V	28.1	17.9	95	24.0	−70.6	−30.4
E665A	−6.6	−16.8	−183	1.0	50.6	−3.9
D519A	−12.4	−13.0	−168	−11.0	143.4	21.8
D519V	−10.4	−9.7	−393	0.6	377.6	5.4
E665V	−4.3	−2.1	−183	7.9	187.4	−7.0

methods has been widely tested in the literature for small molecule drug–receptor interactions, though to less extent on protein–protein complexes [21,22]. Estimation of binding free-energy by computational methods for non-covalently associated protein–protein surfaces is a major challenge due to large fluctuations at the binding surface. Since the experimental data for the mutations at Asp666 is not available, the applicability of the free-energy methods to our current study has been validated by the study of four A2 domain mutants, D519A, D519V, E665A, E665V, for which the experimental mutagenesis data is available. It has been reported in two separate studies that the mutation of Asp519 and Glu665 to either Ala or Val showed general improvement in the FVIIIa thermal stability due to improved binding affinity of A2 domain [11,12]. The Asp519 residue is located at the interface of A1 domain while the Glu665 is located at the interface of A3 domain.

We estimated the $\Delta\Delta G_{BIND}$ of the four mutants by PBSA and GBSA methods. The computed free-energies of A2 domain binding together with the experimental free-energies (calculated based on the published K_d values) is presented in Table 2 as well as Fig. 2. While it is difficult to obtain quantitative comparison between the experimental data and computational energies due to inherent approximations in the implicit solvation models and the complex nature of experimental environment and enzyme kinetics, it is encouraging to see that both GBSA and PBSA methods accurately predict that all four mutants show favorable binding affinity relative to WT structure in qualitative agreement with experimental data [12]. The computational energies are in general several orders of magnitude larger than the corresponding experimental values suggesting that the free-energy calculations systematically overestimate the free-energies (Fig. 2). However, the overall trend of binding energy data is comparable between the experimental and computational methods. The PBSA method accurately predicts that the E665A mutant has the largest binding affinity in line with the corresponding experimental data. In the WT structure, Glu665 forms a salt-bridge with Arg1966 of A3 domain. Mutation of Glu → Ala abolishes the ion-pair. It has been reported in several studies that the salt-bridges in the core of the protein domains destabilize the protein structures due to significant cost of desolvating the two charged salt bridge partners [23,24]. Thus, elimination of the salt-bridges in the E665A or E665V mutants could be attributed to the improvement in the binding affinity of A2 domain. In contrast, the D519A mutant was reported to have least stabilization of binding affinity among the four mutants by experimental studies while both GBSA and PBSA methods rank E665V mutant with the lowest binding affinity. Analysis of the solution structure of E665V reveals that, when compared to WT structure, the Valine side-chain appears to cause some degree of steric repulsion in the surrounding residues. The PBSA method predicts that the mutation lowers the polar and non-polar energy contributions by 7.9 kcal/mol and 187.4 kcal/mol respectively (Table 2). Despite the disagreement in the overall ranking of the relative stabilities, it is important to note that all four mutants are predicted to improve the binding affinity in full agreement with the experimental data and attests to the validity of the WT solution structure and the critical atomic level domain–domain interactions. This is particularly important since the model was derived from the low resolution X-ray crystal structure [13].

3.3. Identification of potential A2 domain residues for mutational study

Analysis of the interface residues of FVIIIa reveals that 27 of the A2 domain residues have interface contacts with A1 domain whereas 16 interface contacts with A3 domain (Tables S1 and S2). While a number of these residues could possibly be ideal targets for improving A2-domain affinity, we focus here on Asp666 residue that interfaces the A3 domain for further analysis. The residue has ~52% of solvent accessibility surface area with sufficient conformational space around the side-chain. As shown in Fig. 1, the location of Asp666 could be very promising since the residue is found to have no potential contacts with neighboring residues of A3 domain, except a hydrogen bond between the side-chain atoms of Asp666 (OD2) and Ser1799 (OG). Moreover, Asp666 is located at the junction of two β-sheets that comprises of residues Val662–Glu665 and Thr667–Leu670. Since Asp666 is not part of any secondary structural regions, the conformational impact of Asp666 mutations on the overall tertiary structure of FVIIIa would be expected to be minimal. This is very critical for maintaining the global structural features of the protein for proper molecular recognition and productive binding with FIXa enzyme. As listed in Table 1, Asp666 residue is not listed in the FVIII mutational

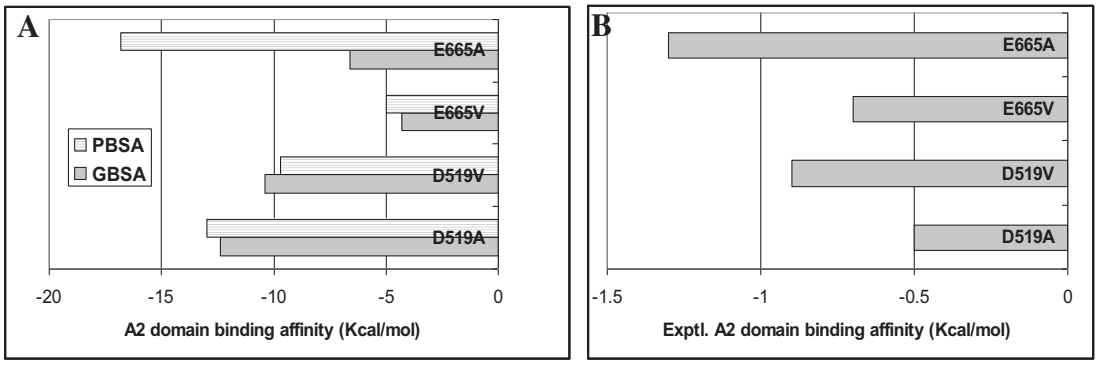

Fig. 2. The computed A2 domain binding free-energies for the mutant structures of Asp519 and Glu665 residues (A) and the corresponding experimental binding free-energies (B). All values are relative to the WT in kcal/mol.

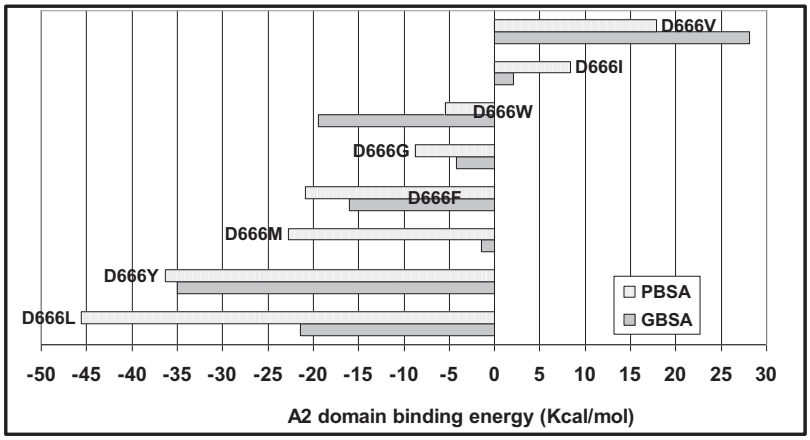

Fig. 3. The computed A2 domain binding free-energies for several hydrophobic mutant structures of Asp666 residue. All values are relative to the WT in kcal/mol.

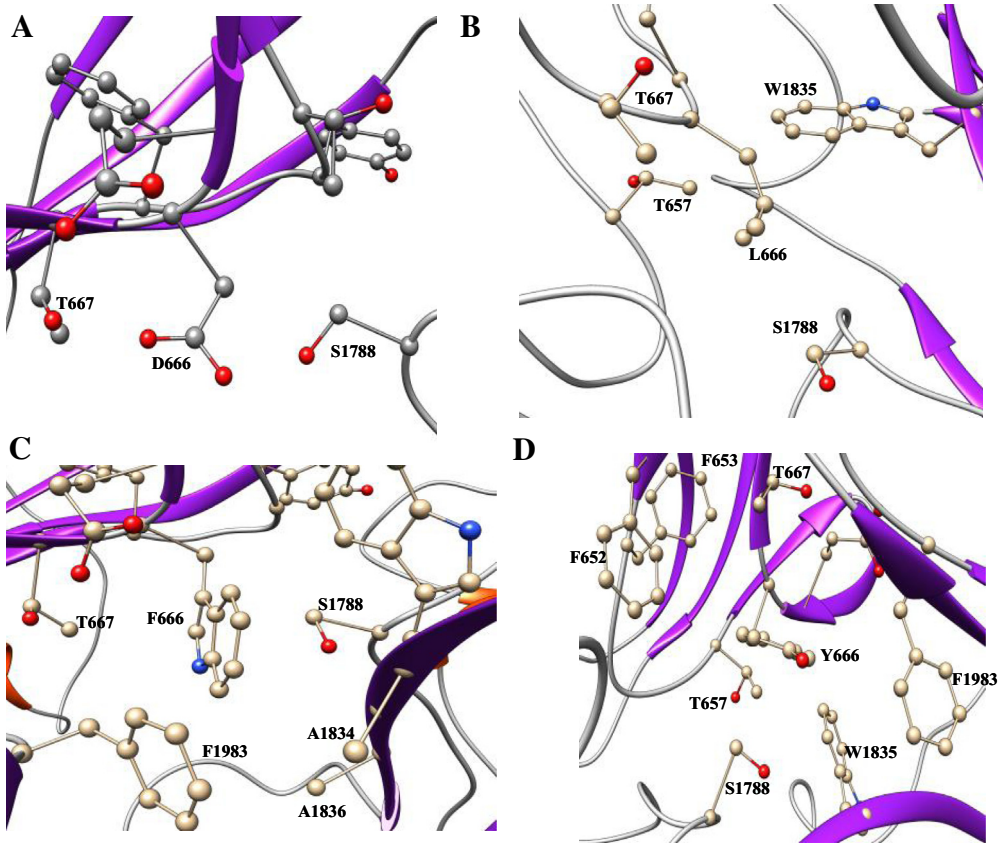

Fig. 4. Residues surrounding the mutant site in MD derived structures of Asp666 (A), Leu666 (B), Phe666 (C) and Tyr666 (D).

database to cause point mutations in patient database and may be considered as a safe modification [4].

3.4. Mutation of Asp666 to hydrophobic residues

We studied the structural effect of eight mutations of Asp666 residue of A2 domain. These mutants are: D666Y, D666L, D666W, D666G, D666V, D666F, D666I and D666M. Each mutant structure was refined for at least 100 ns of MD simulations. The estimated relative $\Delta\Delta G_{BIND}$ values and various components of the free-energy terms by PBSA method are listed in Table 2 as well as in Fig. S2. For comparison, the $\Delta\Delta G_{BIND}$ values by GBSA method are also listed. It is evident from the data that the mutation of Asp666 to Leu, Tyr, Phe, Met, Gly and Trp are well tolerated within the FVIIIa complex. Both GBSA and PBSA methods produced similar trends of energy stability in general while the relative stability of the mutants differs to some extent. Both methods predict Tyr and Leu mutations contribute highest affinity of A2 domain among the eight mutants while the mutation to Valine significantly destabilizes the complex (see Fig. 3).

The equilibrated structures from 120 ns of MD trajectory for four select mutants (WT, Leu666, Phe666 and Tyr666) are shown in Fig. 4 highlighting the surrounding residues. Three aromatic residues Phe652 from A2-domain and Trp1835/Phe1983 from A3 domain form a cluster of hydrophobic patch at the interface with Tyr666 resulting in the stronger stabilization of the A2/A3 domain interface (Fig. 4d). It is not surprising that the Tyr mutation contributes to the stabilization of the complex since aromatic–aromatic

interactions are well-known to improve the binding affinity in protein structures, particularly at the core of the protein structures [25]. Though Phenyl alanine and Tyrosine side-chains are similar except the hydroxyl group of Tyrosine's phenyl moiety, the D666F mutant is relatively less effective in improving the binding affinity than Tyr666 mutation. The D666F mutant, surrounded by Phe1983, Thr667, Ala 1834 and Ala1836, appears to have less favorable electrostatic and Van der Wall's interactions ($\Delta\Delta E_{Gas}$). The PBSA method predicts the D666F mutant destabilizes the FVIIIa complex by ~15 kcal/mol than the Tyr666 mutant. To our surprise, the bulky aromatic side-chain of Tryptophan seems to be not favorable at Asp666 site. The D666W mutant improves the binding affinity by only 5.5 kcal/mol compared to WT. We observe only a marginal improvement in the non-polar and gas-phase energies of D666W mutation. Since D666G mutant stabilizes the A2 domain by ~3 kcal/mol more than D666W mutant suggests that the optimal size of the side-chain of the mutant residues should also be considered as an important factor in designing the new mutants.

The PBSA method predicts the D666L mutant to be energetically more favorable than D666Y mutant, though the GBSA method shows lesser stability than D666Y mutant. Nonetheless both methods are in qualitative agreement in ranking D666L and D666Y mutants as the best possible modifications for Asp666 residue. Analysis of various free-energy components suggest that both gas-phase and dispersion energies are favorable for Leu666 mutant. The side chain of Leu666 maintains hydrophobic interactions with Thr657, Thr667, Trp1935 and Ser1788. These interactions contribute to stronger non-polar and dispersion forces (Table 2).

In conclusion, our data emphasizes the importance of hydrophobic mutations at the Asp666 residue in stabilizing the A2 domain in FVIIIa complex. Given that we are able to reproduce the experimental data on Asp519 and Glu665 mutants with reasonable accuracy, we are confident that our results on hitherto unknown Asp666 mutants warrant further investigation by experimental work. Based on PBSA methodology, we predict that the impact of enhancing the overall A2 domain binding affinity of hydrophobic mutants is in the order of: Leu > Tyr > Met > Phe > Gly > Trp. Our results also suggest that Valine and Ile mutants of Asp666 may not be good candidates for structural modification of FVIIIa.

Acknowledgments

This work was partly supported by the National Institutes of Health Grant (R15-HL082632). The computing resources were acquired by MRI Grant from National Science Foundation (NSF-ACI-1126543). We also thank Professor Philip Fay, University of Rochester Medical center for providing the experimental K_d values.

Appendix A. Supplementary data

Supplementary data associated with this article can be found, in the online version, at http://dx.doi.org/10.1016/j.bbrc.2014.06.043.

References

[1] E.W. Davie, Biochemical and molecular aspects of the coagulation cascade, Thromb. Haemost. 74 (1995) 1–6.
[2] E.W. Davie, K. Fujikawa, W. Kisiel, The coagulation cascade – initiation, maintenance, and regulation, Biochemistry 30 (1991) 10363–10370.
[3] G.A. Vehar, B. Keyt, D. Eaton, H. Rodriguez, D.P. Obrien, F. Rotblat, H. Oppermann, R. Keck, W.I. Wood, R.N. Harkins, E.G.D. Tuddenham, R.M. Lawn, D.J. Capon, Structure of human factor-VIII, Nature 312 (1984) 337–342.
[4] G. Kemball-Cook, E.G.D. Tuddenham, A.I. Wacey, The factor VIII structure and mutation resource site: HAMSTeRS version 4, Nucleic Acids Res. 26 (1998) 216–219.
[5] P.F. Fogarty, Biological rationale for new drugs in the bleeding disorders pipeline, Hematology Am. Soc. Hematol. Educ. Program (2011) 397–404.
[6] J.A. Dumont, T. Liu, S.C. Low, X. Zhang, G. Kamphaus, P. Sakorafas, C. Fraley, D. Drager, T. Reidy, J. McCue, H.W.G. Franck, E.P. Merricks, T.C. Nichols, A.J. Bitonti, G.F. Pierce, H. Jiang, Prolonged activity of a recombinant factor VIII-Fc fusion protein in hemophilia A mice and dogs, Blood 119 (2012) 3024–3030.
[7] E.T. Parker, C.B. Doering, P. Lollar, A1 subunit-mediated regulation of thrombin-activated factor VIII A2 subunit dissociation, J. Biol. Chem. 281 (2006) 13922–13930.
[8] S.W. Pipe, A.N. Eickhorst, S.H. McKinley, E.L. Saenko, R.J. Kaufman, Mild hemophilia A caused by increased rate of factor VIII A2 subunit dissociation: evidence for nonproteolytic inactivation of factor VIIIa in vivo, Blood 93 (1999) 176–183.
[9] B.W. Shen, P.C. Spiegel, C.H. Chang, J.W. Huh, J.S. Lee, J. Kim, Y.H. Kim, B.L. Stoddard, The tertiary structure and domain organization of coagulation factor VIII, Blood 111 (2008) 1240–1247.
[10] J.C.K. Ngo, M. Huang, D.A. Roth, B.C. Furie, B. Furie, Crystal structure of human factor VIII: implications for the formation of the factor IXa-factor VIIIa complex, Structure 16 (2008) 597–606.
[11] H. Wakabayashi, F. Varfaj, J. DeAngelis, P.J. Fay, Generation of enhanced stability factor VIII variants by replacement of charged residues at the A2 domain interface, Blood 112 (2008) 2761–2769.
[12] H. Wakabayashi, P.J. Fay, Identification of residues contributing to A2 domain-dependent structural stability in factor VIII and factor VIIIa, J. Biol. Chem. 283 (2008) 11645–11651.
[13] D. Venkateswarlu, Structural investigation of zymogenic and activated forms of human blood coagulation factor VIII: a computational molecular dynamics study, BMC Struct. Biol. 10 (2010) 7.
[14] E.F. Pettersen, T.D. Goddard, C.C. Huang, G.S. Couch, D.M. Greenblatt, E.C. Meng, T.E. Ferrin, UCSF chimera – a visualization system for exploratory research and analysis, J. Comput. Chem. 25 (2004) 1605–1612.
[15] R. Salomon-Ferrer, A.W. Gotz, D. Poole, S. Le Grand, R.C. Walker, Routine microsecond molecular dynamics simulations with AMBER on GPUs. 2. Explicit solvent particle mesh Ewald, J. Chem. Theory Comput. 9 (2013) 3878–3888.
[16] D. Case, T. Darden, T. Cheatham III, C. Simmerling, J. Wang, R. Duke, R. Luo, R. Walker, W. Zhang, K. Merz, AMBER 12, University of California, San Francisco, 2012.
[17] H. Nguyen, D.R. Roe, C. Simmerling, Improved generalized born solvent model parameters for protein simulations, J. Chem. Theory Comput. 9 (2013) 2020–2034.
[18] C. Tan, Y.-H. Tan, R. Luo, Implicit nonpolar solvent models, J. Phys. Chem. B 111 (2007) 12263–12274.
[19] B.R. Miller, T.D. McGee, J.M. Swails, N. Homeyer, H. Gohlke, A.E. Roitberg, MMPBSA.py: an efficient program for end-state free energy calculations, J. Chem. Theory Comput. 8 (2012) 3314–3321.
[20] S. Hubbard, NACCESS: program for calculating accessibilities, 1992.
[21] I. Massova, P.A. Kollman, Combined molecular mechanical and continuum solvent approach (MM-PBSA/GBSA) to predict ligand binding, Perspect. Drug Discovery Des. 18 (2000) 113–135.
[22] T. Hou, J. Wang, Y. Li, W. Wang, Assessing the performance of the MM/PBSA and MM/GBSA methods. 1. The accuracy of binding free energy calculations based on molecular dynamics simulations, J. Chem. Inf. Model. 51 (2011) 69–82.
[23] Z.S. Hendsch, B. Tidor, Do salt bridges stabilize proteins – a continuum electrostatic analysis, Protein Sci. 3 (1994) 211–226.
[24] F.B. Sheinerman, B. Honig, On the role of electrostatic interactions in the design of protein–protein interfaces, J. Mol. Biol. 318 (2002) 161–177.
[25] S.K. Burley, G.A. Petsko, Aromatic–aromatic interaction – a mechanism of protein-structure stabilization, Science 229 (1985) 23–28.